Journal of Geodetic Science

• 2(2) • 2012 • 107-112 DOI: 10.2478/v10156-011-0031-x •

Polyaxial figures of the Moon from the lunar reconnaissance orbiter laser altimetry and multi-mission synthesis of the lunar shape

Research Article

H. Bâki İz[1]*, C.K. Shum[2], C.L. Dai[2]

1 *Dept. of Land Surveying and Geo-Informatics, The Hong Kong Polytechnic University, Hong Kong, China*
2 *Division of Geodetic Science, School of Earth Sciences, The Ohio State University, USA*

Abstract:
Last decade witnessed a plethora of missions to the Moon by China (Chang'E-1 and Chang-E-2), Japan (SELenological and ENgineering Explorer, SELENE), India (Chandrayaan-1) and USA (Lunar Reconnaissance Orbiter), all carried out laser altimetry measurements. This study is a follow up to a series of earlier investigations that produced a number of new models to represent the gross geometric shape of the Moon using Unified Lunar Control 2005, Chang'E-1, and SELENE laser altimetry data using the Lunar Reconnaissance Orbiter laser altimetry measurements. The symmetric and asymmetric polyaxial geometric models derived from Lunar Reconnaissance Orbiter laser altimetry data, namely, three, four and six-axial lunar figure parameters, are compared and contrasted with the corresponding model parameters estimated from the Chang'E-1 and SELENE laser altimetry. All solutions produced geometric shape, orientation parameters, and the parameters of the geometric center of lunar figure with respect to the center of mass of the Moon showing remarkable agreement with each other within 100 m. A combined solution by the fusion of uniformly sampled laser altimetry data from all three missions produced the best estimates for the lunar shape, orientation, and lunar center of figure parameters, and their realistic error estimates.

Keywords:
Chang'E-1 • Lunar Laser Altimetry • Lunar Orientation • Lunar Reconnaissance Orbiter • Polyaxial Lunar Figure • Selenological and Engineering Explorer

Received 2012-04-01; accepted 2012-04-18

1. Introduction

Last decade witnessed a plethora of missions to the Moon by Chang'E-1 and Chang-E-2 (China), SELenological and ENgineering Explorer, SELENE (Japan), Chandrayaan-1 (India) and Lunar Reconnaissance Orbiter, (LRO) (USA), all carried out laser altimetry measurements. These measurements can be used to map the lunar surface and investigate the lunar shape.

Spherical figures are the first order approximations to the gross shape of the Moon. Symmetrical two-axial (rotational) or three-axial ellipsoids approximate the Moon's hydrostatically stable axisymmetric figure. Lunar shape is also described in combination with lunar topography by a sufficiently high degree and order spherical harmonic topographic model (Ping et al., 2009, Araki et al., 2009) and the deviations from the symmetry can be deduced from low degree and order harmonic coefficients of such solutions. Iz et al. (2011a) has shown that asymmetric ellipsoids can also serve as alternative models.

Iz (2009) initiated the first comprehensive computation of the parameters of the geometrically best fitting two-axial and three-axial ellipsoids, and spheres from the coordinates of 271,610 Unified Lunar Control Network's, (ULCN 2005) (Archinal et al., 2006) lunar control stations. Subsequently, Iz et al. (2009b) showed that the complete omission of the topography in the old Unified Lunar Control Networks (ULCN 1994) solution shifted the geometric center of the

*E-mail: lshbiz@polyu.edu.hk

lunar figure up to 5 km in the lunar equatorial plane and rotated the ULCN 1994 reference frame with respect to ULCN 2005 reference frame on the order of few hundred meters (on the lunar equator).

Iz et al.'s (2010a) study introduced the first estimates for the orientation of the geometrically best fitting triaxial lunar ellipsoid with respect to the Mean/Polar axis reference frame. Iz et al.'s (2011c) study assessed the consistency of Chang'E-1 and SELENE reference frames using nearly colocated laser altimetry footprint positions. Improved, spherical two and three-axial lunar figure parameters together with their geometric centers with respect to the center of mass of the Moon were also calculated, using Chang'E-1 and SELENE laser altimetry data by Iz et al. (2011b). Most recently, Iz et al., (2011a) introduced new polyaxial symmetric and asymmetric ellipsoidal models to represent the geometric figure of the Moon and demonstrated that the figure of the Moon can be parsimoniously represented by an egg-shape with only three parameters centered at the lunar center of mass.

The present contribution is a follow up to these earlier investigations that produced a multitude of new models to represent the gross geometric shape of the Moon using the most recent LRO laser altimetry data to validate the earlier models and their solutions.

In the following sections, the symmetric and asymmetric polyaxial geometric model parameters are derived using LRO laser altimetry data namely, three, four and six-axial lunar figure parameters together with their center of figure coordinates with respect to the center of mass of the Moon. These are compared and contrasted with the model parameters estimated from the Chang'E-1 and SELENE laser altimetry measurements (ibid).

The present contribution also provides a combined solution through fusion of all three missions' uniformly sampled laser altimetry data, which produced the best estimates for the lunar shape, orientation, and lunar center of figure parameters for various models, and their realistic error estimates by virtue of statistically independent data from the three lunar missions.

2. Lunar Laser Altimeter Data from Chang'E-1, SELENE and LRO Missions

Chang'E-1 was launched on October 24, 2007. The satellite orbited around the Moon in an approximately 2-hour polar orbit with an inclination of $90^\circ \pm 2^\circ$ at an altitude about 200 km. The footprint size of the laser spot produced by the onboard laser altimetry system was typically 100 m at this altitude. The along-track data spacing was about 1.4 km. *China Lunar Exploration Center* provided the footprint locations of over 8.5 million selenocentric laser altimetry measurements (after removing over 300,000 outliers) for this study. The radial distances of the laser altimetry footprints were calibrated by comparing them against the radial distances of the Lunar Laser Ranging sites (Iz, et al. 2011b).

Japan Aerospace Exploration Agency (JAXA) launched SELENE on 14 September 2007. The main satellite (KAGUYA) orbited around the Moon at an altitude of 100 km ±30 km above the lunar surface with an inclination of $90^\circ \pm 1^\circ$ and approximately 2-hour period. The footprint size was typically 40 m, and the data spacing was about 1.6 km in along-track direction (Araki et al., 2009). *JAXA* (2009) provided over 8.8 million selenocentric SELENE laser altimetry measurements and their footprint locations. Statistical analysis of the laser altimetry footprint positions nearby the *Lunar Laser Ranging* station coordinates did not show any statistically significant differences (ibid). Hence, no calibration correction was applied to the SELENE laser altimetry footprint radial distances.

LRO was launched on June 18, 2009. The satellite orbited around the Moon at an altitude of 190 km initially and down to approximately 50 km above the lunar surface with polar orbit. LRO laser altimeter can perform off-nadir observations as compared to the other altimeters of the other two missions which can only make nadir measurements. Each single laser measurement contains five output beams with each beam (i.e. footprint) size of 5 m and the separation of each beam is 25 m. At 50-km altitude, off-nadir pointing can move the laser altimeter swath on the surface by 50 or 100 m. Overall, the data spacing was approximately 56 m in along-track direction with current across-track separation at approximately 1.8 km as a result of an laser altimetry data acquisition rate between 80 and 90 measurements per second (Smith et al., 2010). The orbiter produced over 1.1 billion laser altimetry measurements between June 18, 2009 and August 10, 2011. The precision of laser altimetry measurements are within ± (1-5) m range for various measurement systems.

Laser altimetry measurements by different missions are all referenced to the Mean Earth/Polar axis reference system.

3. Solutions for the Polyaxial Geometric Figures of the Moon

An irregular geometric representation of the lunar figure by an asymmetric polyaxial model is shown in Fig. 1. The principal axes *a* and *a'* are the equatorial axes along the *X*-axis of the Mean Earth/Polar axis reference system on the nearside and the far side, *b*, and *b'* are the other equatorial axes parallel to the *Y*-axis, and *c*, and *c'* are the polar axes parallel to the *Z*-axis . The position of the geometric center of the polyaxial figure, the shift parameters with respect to the center of mass of the Moon that coincides with the origin of the Mean Earth/Polar axis reference system, is denoted by x_c, y_c, z_c. The six axes divide the asymmetric geometric figure of the Moon into *eight quadrants* where each quadrant can be represented by a triaxial ellipsoid using the following mathematical model (Iz, et al., 2011a)

$$(R\Delta x)^T S\,(R\Delta x) - 1 = 0 \qquad (1)$$

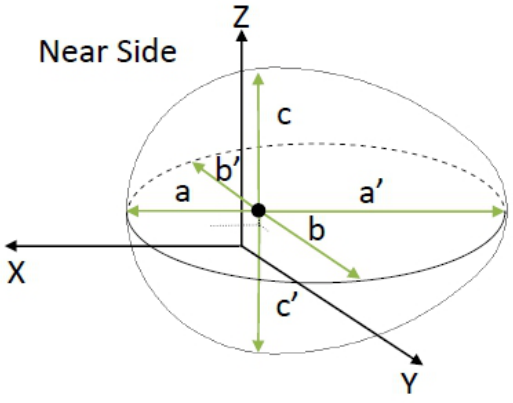

Figure 1.

where,

$$R := \begin{pmatrix} 1 & 0 & 0 \\ 0 & \cos\alpha & \sin\alpha \\ 0 & -\sin\alpha & \cos\alpha \end{pmatrix} \begin{pmatrix} \cos\beta & 0 & -\sin\beta \\ 0 & 1 & 0 \\ \sin\beta & 0 & \cos\beta \end{pmatrix} \begin{pmatrix} \cos\gamma & \sin\gamma & 0 \\ -\sin\gamma & \cos\gamma & 0 \\ 0 & 0 & 1 \end{pmatrix} \quad (2)$$

$$\Delta x := \begin{pmatrix} x - x_c \\ y - y_c \\ z - z_c \end{pmatrix}, \quad S := \begin{pmatrix} \mathrm{a}^{-2} & 0 & 0 \\ 0 & \mathrm{b}^{-2} & 0 \\ 0 & 0 & \mathrm{c}^{-2} \end{pmatrix}, \quad (3)$$

in which α, β, γ are the *common* rotation angles of the lunar figure about the X, Y, Z axes respectively and S is the lunar shape matrix consisting of principal axes that conform with the axes of the corresponding quadrant (i.e. a is replaced with a′, b with b′ and c with c′). In this formulation, having common axes between quadrants ensures that the transition from one quadrant to another is smooth (no jumps).

This model also serves as a condition equation for the *non-linear* statistical model of the laser altimetry measurements. It is solved for the unknown shape, orientation, and shift parameters of the lunar figure from the Cartesian coordinates of the laser altimetry footprints from Chang'E-1 and SELENE and LRO missions using the method of least squares for *the condition equations with unknown parameters* iteratively discussed in Iz, (2009).

In estimating lunar shape parameters modeling each quadrant enables capturing the effect of the regional scale topographical features such as South Pole-Aitken region, one of the largest topographical features in the solar system, and highlands of the Eastern part on the far side.

Additional sub-models are obtained by removing shape parameters that are not significantly different from each other. Because of the large number of data used in the solutions, all null-hypothesis testing for the differences in the shape parameters are rejected (i.e. all the estimated parameters are found to be statistically significant from their counterparts, such as $\mathrm{a} \neq \mathrm{a}'$, $\mathrm{b} \neq \mathrm{b}'$, $\mathrm{c} \neq \mathrm{c}'$), hence such tests are of limited use for model comparison and selection. Instead, misclosures, deviations from 1 in the condition equations with unknown parameters shown in eq. 1, can be used to assess the impact of model parameters and eliminate those that are not contributing to the solutions.

Laser measurements from all missions were carried out by satellites in near polar orbits resulting in an uneven distribution of data, increasingly denser toward the lunar poles, which create correlation among the solution parameters. To minimize such correlations as well as to provide a homogeneous set of data to be used for comparisons among different data sets, 250,000 uniformly distributed laser altimetry measurements were selected using the random sampling approach on a unit sphere discussed by Iz et al. (2011b) from each mission's repository. Separate solutions were obtained to validate the solutions obtained from Chang'E-1, SELENE laser altimetry data with the solutions calculated from the LRO laser altimetry.

Table 1 lists the estimates from various geometric models of the Moon. These models either include the center of figure parameters or ignore them in solving the gross shape parameters (such models are differentiated by titles; models *with* and *without* center of figure parameters). In this table, the solutions are listed first for the Chang'E-1, then SELENE and LRO laser altimetry data, followed by the combination solution that includes all the data from the three lunar missions. Common to all solutions is the principal axes of the ellipsoids that remain parallel to the underlying mean Earth/polar axis reference frame (i.e. the rigid body rotations of the ellipsoids are constrained to be zero as opposed to solutions to models with *the rotation angles* given in Table 2).

The standard errors of the estimates show very precise estimates, less than 1m for the principal axes and the geometric center parameters. Yet, the standard errors do not reflect the accuracy of the estimated parameters since the expected value of the residual lunar topography is not zero, which leads to biased estimates for the parameters and their standard deviations are only a measure of precision. Although Chang'E-1 and SELENE solutions are both calibrated against the coordinates of the near side lunar laser ranging sites (Iz et al., 2011b), calibration ensures the accuracy of the laser altimetry footprint coordinates confined only to the near-side of the Moon including the LRO data. However, each mission's laser altimetry measurements are completely independent from each other. Therefore, biased estimates from each mission tend to exhibit random excursions from mission-to-mission solutions and their average values are expected to provide the best estimates for the relevant parameters. The dispersion of the parameters from their averaged values should also provide better accuracy estimates for the solution parameters. Meanwhile, a better alternative to simple averaging the estimates is to obtain the new

Table 1. All units are in m. Three, four and six-axial lunar shapes *with* and *without* center of figure parameters from the Chang'E-1,SELENE and LRO laser altimetry data. The first three rows for each axis are for Chang'E-1, SELENE, and LRO solutions, followed by the combined solution from all missions. (S) denotes an axially symmetric model. RMS Δ are the RMS values of the difference between the combined solution and each mission solution in meters. RMS Misc are the RMS misclosures (deviations from 1) scaled by an average radius of the Moon.

Principal Axes	Three-axial (S) a, b, c		Three-axial a, a', c	Four-axial a, a', b, c			Six-axial a, a', b, b', c, c'	
a	1738027	1738022	1736959	1737634	1735862	1737856	1735862	1737856
	1738085	1738070	1736988	1737671	1735881	1737793	1735882	1737793
	1737959	1737950	1736930	1737596	1735852	1737853	1735853	1737855
	1738022	1738014	1736959	1737633	1735865	1737834	1735865	1737835
a'			1740396	1738372	1740178	1738188	1740179	1738187
			1740473	1738447	1740254	1738345	1740254	1738346
			1740253	1738259	1740039	1738047	1740041	1738046
			1740374	1738359	1740157	1738193	1740158	1738193
b	1737613	1737615			1737618	1737615	1736689	1737028
	1737646	1737661			1737652	1737660	1736722	1737088
	1737568	1737574			1737577	1737574	1736717	1737157
	1737609	1737616			1737616	1737616	1736709	1737092
b'							1738538	1738200
							1738597	1738234
							1738428	1737990
							1738521	1738141
c	1735684	1735686	1735683	1735685	1735684	1735685	1736002	1736395
	1735699	1735691	1735698	1735691	1735697	1735691	1736028	1736461
	1735836	1735837	1735837	1735837	1735837	1735837	1736069	1736402
	1735739	1735738	1735739	1735738	1735739	1735738	1736033	1736420
c'							1735369	1734977
							1735356	1734919
							1735607	1735273
							1735445	1735056
x_c		-1718		-1441		-1593		-1594
		-1736		-1445		-1529		-1528
		-1670		-1422		-1598		-1599
		-1708		-1436		-1573		-1574
y_c		-710		-710		-710		-270
		-721		-721		-721		-291
		-663		-663		-663		-351
		-698		-698		-697		-304
z_c		217		217		217		-314
		230		230		230		-348
		157		156		157		-267
		201		201		201		-310
RMS Δ	53	43	68	52	59	59	47	81
RMS Misc	4300	3727	3924	3727	3846	3726	3750	3722

parameters using the combined data from all three missions and to use the parameters of the combined solutions instead.

In pursuing this premise, the fourth solution listed in Table 1 shows the parameters from the combined solutions. Table 1 also includes the root mean square (RMS) values of the differences between the combined solution, and each mission solution parameters in meters. They provide a better estimate for the accuracy of the combined solution estimates for each model.

The results show that the RMS differences are consistent from model to model, which suggest that each mission solution parameters agree approximately within 50 m, only showing a large RMS differences among different solution parameters for the polyaxial solution with nine parameters (the last column). This difference suggests that the model parameters from different missions deviate at regional scales, revealing the presence of systematic errors of different mission solutions in representing the long wavelength features of the lunar topography.

The RMS values of the misclosures for the combined solution are also included in Table 1. Misclosures are the deviations from unity in eqn 1 scaled by an average radius of the Moon to provide a

Table 2. Three, four and six-axial lunar shapes *with* and *without* center of figure parameters (m) and *with* and *without* orientation parameters (degrees) from the Chang'E-1 SELENE and LRO laser altimetry data. The first three rows for each axis are for Chang'E-1, SELENE, and LRO solutions, followed by the combined solution from all missions. (S) denotes an axially symmetric model. RMS Δ are the RMS values of the difference between the combined solution and each mission solution in meters. RMS Misc are the RMS misclosures (deviations from 1) scaled by an average radius of the Moon. RMS Δs do not include the differences in the orientation parameters between different solution and the combined solution.

Principal Axes	Three-axial (S) a, b, c		Three-axial a, a', c		Four-axial a, a', b, c		Six-axial a, a', b, b', c, c'	
a	1739022	1739024	1737040	1737340	1736517	1737224	1736502	1737469
	1739092	1739088	1737072	1737375	1736547	1737277	1736531	1737557
	1738891	1738887	1737024	1737333	1736500	1737263	1736495	1737470
	1739002	1738999	1737045	1737349	1736522	1737255	1736510	1737498
a'			1741591	1740707	1741487	1740779	1741476	1740565
			1741682	1740791	1741578	1740851	1741569	1740621
			1741331	1740426	1741227	1740470	1741216	1740296
			1741534	1740641	1741430	1740700	1741420	1740494
b	1737339	1737338			1737353	1737362	1737584	1739195
	1737365	1737370			1737386	1737394	1737615	1739247
	1737323	1737324			1737338	1737346	1737530	1738913
	1737342	1737343			1737359	1737367	1737577	1739119
b'							1737148	1735379
							1737181	1735379
							1737164	1735633
							1737163	1735461
c	1734961	1734963	1734971	1734963	1734973	1734964	1734938	1739265
	1734974	1734969	1734978	1734970	1734980	1734970	1734963	1739418
	1735147	1735149	1735159	1735148	1735161	1735149	1735037	1738991
	1735028	1735027	1735036	1735028	1735038	1735028	1734979	1739224
c'							1735008	1730786
							1734998	1730647
							1735283	1731426
							1735097	1730955
x_c		-1718		-695		-638		-1382
		-1736		-697		-648		-1431
		-1669		-726		-692		-1388
		-1708		-706		-660		-1399
y_c		-714		-187		-157		-1686
		-723		-191		-165		-1725
		-666		-184		-166		-1452
		-701		-187		-162		-1622
z_c		220		-97		-113		-3239
		226		-91		-104		-3332
		157		-138		-148		-2938
		201		-108		-122		-3169
α	17.46	17.53	19.10	19.91	19.40	19.93	18.67	9.53
	17.20	17.39	18.85	19.70	19.15	19.71	18.47	9.38
	18.22	18.44	19.84	20.73	20.18	20.74	19.36	10.40
	17.61	17.77	19.25	20.10	19.56	20.10	18.81	9.74
β	21.35	21.35	17.41	18.43	16.88	18.32	16.30	22.26
	21.39	21.24	17.32	18.32	16.79	18.22	16.20	22.22
	21.65	21.54	17.36	18.70	16.77	18.63	16.45	22.44
	21.46	21.37	17.36	18.48	16.82	18.38	16.31	22.30
γ	27.03	27.19	31.10	33.89	31.87	33.91	33.96	31.03
	26.78	27.33	30.91	33.71	31.65	33.72	33.72	30.96
	26.84	27.18	30.57	33.51	31.30	33.53	33.08	31.00
	26.89	27.24	30.86	33.70	31.61	33.72	33.60	31.00
South Pole Comb. Sol.	62.51S 165.94E	62.42S 165.98E	64.30S 161.38E	62.94S 164.63E	64.42S 160.76E	63.00S 164.49E	65.29S 163.09E	65.76S 186.78E
RMS Δ	69	54	100	83	87	72	54	166
RMS Misc	3976	3348	3346	3297	3325	3297	3322	3117

commensurable quantity for assessing the goodness-of-fit. Misclosures, by their very nature, include the random errors in the measurements and the unmodeled topography in this particular exercise. The RMS misclosures are smaller with increasing complexity of each model (larger number of parameters) as expected (confer to Iz et al. 2011a for additional discussion on this issue).

Model solutions that also include lunar figure orientation parameters are listed in Table 2. The RMS differences between the combined solutions of individual mission solutions are larger than the solutions *without* the orientation parameters but consistent from model to model reveal that solutions with orientation parameters are sensitive to large-scale lunar topography. The RMS misclosures are smaller as compared to the solutions *without* orientation parameters. This is due to the additional flexibility for the least squares solutions, which is provided with increased number of parameters via modeling the orientation of the lunar figure with respect to the Mean Earth/Polar axis reference system.

Table 2 also includes the estimates for the latitudes and longitudes of the lunar South Pole position of the polar axes of various model solutions. Again, it is evident that the solutions *with* the orientation angles, as also confirmed by the most recent mission LRO solution parameters in this study, are dominated by the South Pole-Aitken impact region, the largest known topographical feature in the solar system. As a result, the position of the South Polar axis in all solutions located within the South Pole-Aitken region becomes close to the center of its elliptical shape.

4. Conclusion

LRO solutions validated earlier solutions and models based on Chang'E-1 and SELENE laser altimetry data (Iz, et al., 2011a).

Overall, the results show that the lunar figure can be represented equally well by different models; each one of these models is informative in their own way. Constrained models, i.e. those *without* orientation parameters are more consistent with each other.

The syntheses of the three mission data via combination solutions for different models provide the best estimates for the lunar shape, center of figure and orientation parameters. The error estimates inferred from the RMS differences of each mission solution parameters from the combined solution parameters are dominantly less than 100 m. They are more realistic representation of the errors of the estimated parameters.

Acknowledgements

This study is supported by the Hong Kong Polytechnic University Central Research Grant G.34.27.YJ77. The Ohio State University component of the study is supported by NASA's Lunar Advanced Science and Exploration Research (LASER) Program (Grant No. NNX11AC53G). We acknowledge Japan Aerospace Exploration Agency's (JAXA's) SELENE project, Chang'E-1 project and National Aeronautical Space Agency's (NASA) LRO project for providing the lunar data products used in this study. We are grateful for the prompt and insightful comments from two anonymous reviewers.

References

Araki H., Tazawa S., Noda H., Ishihara Y., Goossens S., Sasaki S., Kawano N., Kamiya I., Otake H., Oberst J. and Shum C. , 2009, Lunar global shape and polar topography derived from Kaguya-LALT laser altimetry, Science, 323, 898-900.

Archinal B.A., Rosiek M.R., Kirk R.L. and Redding B.L., 2006, The unified lunar control network 2005: U.S. Geological Survey Open-File Report 2006-1367,http://pubs.usgs.gov/of/2006/1367/.

Iz H.B., Ding X.L., Shum C.K. and Dai C.L., 2011, Polyaxial Figures of the Moon, J Geod. Sci., 1, 4, 348-354.

Iz H.B., Shum C.K., Chen Y.Q. and Dai C.L., 2011, An Improved geometrically best fitting lunar figure from Chang'E-1 and SELENE laser altimetry, J Appl. Geod., 5, 1-12.

Iz H.B., Chen Y.Q., Ding X.L., King B.A., Shum C.K., Wu C. and Berber M., 2011, Assessing consistency of Chang'E-1 and SELENE reference frames using nearly-colocated laser altimetry footprint positions, J Geod., 86, 109-117.

Iz H.B., Shum C.K., Ding X.L. and Dai C.L., 2010, Orientation of the geometrically best fitting triaxial lunar ellipsoid with respect to the mean Earth/Polar axis reference frame, J Geod. Sci., 1, 1, 52-58.

Iz H.B., Chen Y.Q., King B.A., Ding X.L. and Wu C., 2009, Deformation analysis of the unified lunar control networks, J Appl. Geod., 3, 231-238.

Iz H.B., 2009, New parameters of geometrically best fitting lunar figures, J Appl. Geod., 3, 155-162.

JAXA, https://www.soac.selene.isas.jaxa.jp/archive/index.html.en, 2009.

Ping J., Huang Q., Shu R. and Yan J., 2009, Lunar topography result from Chang'E-1 laser altimetry mission, presented at the 3rd KAGUYA(SELENE) science working team meeting, Tokyo.

Smith D. E., Zuber M. T., Neumann G. A., Lemoine F. G., Mazarico E., Torrence M. H., McGarry J. F., Rowlands D. D., Head J. W., Duxbury T. H., Aharonson O., Lucey P. G., Robinson M. S., Barnouin O. S., Cavanaugh J. F., Sun X., Liiva P., Mao D., Smith J. C., and Bartels A. E., 2010, Initial observations from the lunar orbiter laser altimeter (LOLA), Geophys. Res. Lett., 37, L18204, Doi:10.1029/2010GL043751.